

# The Influence of Synthesis Parameters on Microstructures and Superconducting Properties of MgB<sub>2</sub> Bulks

Y. F. Wu<sup>a,b,\*</sup> Y. Feng<sup>a</sup> G. Yan<sup>a</sup> J. S. Li<sup>b</sup> H. P. Tang<sup>a</sup>  
 S. K. Chen<sup>a</sup> Y. Zhao<sup>c</sup> M. H. Pu<sup>c</sup> H. L. Xu<sup>a</sup> C. S. Li<sup>a</sup>  
 Y. F. Lu<sup>a</sup>

<sup>a</sup>*Northwest Institute for Nonferrous Metal Research, P. O. Box 51, Xian, Shaanxi 710016, P. R. China*

<sup>b</sup>*Northwestern Polytechnical University, Xi'an 710012, P.R.China*

<sup>c</sup>*Southwest Jiaotong University, Si Chuan 610031, P.R.China*

---

## Abstract

We succeeded in the synthesis of high- $J_c$  MgB<sub>2</sub> bulks via high energy ball-milling of elemental Mg and B powder at ambient temperatures. Alternatively to long-time mechanical alloying technique, the mixed powder was ball-milled for only 1h and the completed reaction is achieved by subsequent annealing. The correlations among synthesis parameters, microstructures and superconducting properties in MgB<sub>2</sub> bulks were investigated. Samples were characterized by XRD and SEM, and the magnetization properties were examined in a SQUID magnetometer. The high- $J_c$ , approximately  $1.7 \times 10^6$  A/cm<sup>2</sup> (15K, 0.59T), and improved flux pinning were attribute to a large number of grain boundaries provided by small grain size.

*Key words:* bulk MgB<sub>2</sub>, high energy ball-milling, high- $J_c$ , flux pinning

*PACS:* 74.70.Ad, 74.62.Bf, 74.25.Qt, 74.25.Sv, 74.50.+r, 74.70.-b

---

## 1 Introduction

The improvement of the intrinsic properties of MgB<sub>2</sub> was recognized as a decisive goal to enable potential applications [1]. Now, MgB<sub>2</sub> is showing higher

---

\* Corresponding author. Tel:+86-29-86231079; fax:+86-29-86224487  
*Email address:* wyf7777@tom.com (Y. F. Wu).

$H_{c2}$  than that of conventional NbTi and Nb<sub>3</sub>Sn and becoming the first promising metallic superconductor applicable at 20K. In particular, very high upper critical field,  $H_{c2}(0)$ , exceeding 30T has been reported for MgB<sub>2</sub> wires, tapes and bulks. However, it was recognized that the irreversibility field  $H_{irr}(T)$  of the samples prepared by standard solid state reaction is apparently lower than  $H_{c2}$  due to weak flux pinning. A typical relationship,  $H_{irr}(T) \sim 0.5H_{c2}(T)$ , has been observed for the undoped MgB<sub>2</sub> bulks [2,3]. It was also shown that for MgB<sub>2</sub>, contrast to high  $T_c$  superconductors, grain boundaries in MgB<sub>2</sub> are not acting as impediments for superconducting currents [1,4]. Unfortunately, a rapid drop of  $J_c$  at high fields, probably related to weak-link-like behavior, can be seen in most studies [5,6,7,8,9,10]. The predominant pinning mechanism in MgB<sub>2</sub> is still controversy. However, a microstructure with very small-sized defects (e.g. grain boundary) should be favorable for the optimum pinning of magnetic flux lines. The high energy ball-milling technique facilitates the formation of an optimal microstructure with small particle sizes. Hence, a high grain boundary density is obtained, which is expected to enhance the magnetic flux pinning ability and to improve the critical currents in external magnetic fields.

## 2 Experimental

In this study Mg(99.8%) and amorphous B(95+%) powders with 5wt% Mg surplus were filled under purified Ar-atmosphere into an agate milling container and milling media. The milling was performed on a SPEX 8000M mill for 1h using a ball-to-powder mass ratio of 3. The milled powders were then cold pressed to form pellets with a diameter of 20mm and a height of 3mm. The pellets were placed in an alumina crucible inside a tube furnace under ultra-high purity Ar-atmosphere. The samples were heated at different temperatures for different times, then cooled down to the ambient temperature.

A Quantum Design SQUID magnetometer was used to measure the AC magnetic susceptibility of the samples over a temperature range of 5 to 50 K under an applied field of 1Oe. Magnetization versus magnetic field (M-H) curves were also measured on rectangular-shaped samples at temperatures of 10 and 15K under magnetic fields up to 90000Oe to determine the critical current density  $J_c(H)$ .

The phase compositions of the samples were characterized by the APD1700 X-ray diffraction instrument. The surface morphology and microstructures of the samples were characterized by the JSM-6460 and the JSM-6700F scanning electron microscope.

### 3 Results and discussion

#### 3.1 The influence of sintering temperature to the phase composition, microscopy and superconducting properties of bulk $MgB_2$

The X-ray diffraction patterns of  $MgB_2$  bulks sintered at different temperatures are shown in figure 1. For the samples sintered at 650 °C, 700 °C and 750 °C, almost single phase  $MgB_2$  appears in the patterns with minor fraction of MgO. The percentage of MgO is apparently increased for the sample sintered at 800 °C, indicating easy oxidation of Mg at higher temperature.

Shown in Fig.2(a) is the surface morphology of the sample sintered at 650 °C. Well-developed coarse columnar grains can be seen in the figure. Evidently, it could not connect very well in the surface. There are also some black impurity phases for the sample sintered at 650 °C, see Fig.2(b). The energy spectrum analysis showed that the black one is the B-rich phase, which is due to the stability of the higher borides at lower temperature, see Fig.3. In contrast, the grains of the samples sintered at 700 °C and 750 °C are equiaxial, fine and well-connected, shown in Fig.2(c) and Fig.2(e). Additionally, there are only a few impurity phases for these samples, see Fig.2(d) and Fig.2(f). It exhibits the sintering temperatures are appropriate right here. A broad grain size distribution can be seen for the sample sintered at 800 °C, as shown in Fig.2(g). The large number of existing impurity phases, see Fig.2(h) would obviously take bad effect to the grain connectivity and lower the superconducting properties of the sample. It is clearly not the suitable temperature for preparation of bulk  $MgB_2$ .

Fig.4 shows the AC magnetic susceptibility as a function of the temperature for the samples sintered at different temperatures. A constant magnetic field of 1Oe was applied. As we can see, all samples have sharp transitions. But it is interesting that the superconducting transition of the samples sintered at 700 °C, 750 °C and 800 °C ( $T_c \sim 1.5$  K) is about 2.5 times sharper than that of the samples sintered at 650 °C ( $T_c \sim 4$  K). It is not clear what caused the transition broaden. However, the broadening could be related to microstructural changes induced by the heat treatment temperature. It seems that the columnar grains lead to worse grain connectivity than the impurity phases.

The magnetization curves (M-H) for the samples sintered at different temperatures are shown in Fig.5.  $J_c(H)$  was determined by Bean critical state model, as shown in Fig.6. The  $J_c$  at 0K is nearly equal for all the samples. However, the sample sintered at 750 °C has a significantly higher  $J_c$  than the other samples in magnetic field, indicating improved magnetic flux pinning of it. The differences in  $J_c$  among them increase with field. The sample sintered

at 650 °C shows a steep drop in  $J_c$  at higher fields ( $H > 4T$  and  $T = 10K$ ). It is most probably because of the columnar grains existing in the sample lead to bad grain connectivity, which severely limits its  $J_c$  performance. No such steep drop in  $J_c$  is observed for the other samples.

### 3.2 *The influence of the holding time to the phase composition, microscopy and superconducting properties of bulk MgB<sub>2</sub>*

The X-ray diffraction patterns of bulk MgB<sub>2</sub> sintered for different times are shown in figure 7. Mainly peaks of MgB<sub>2</sub> are visible but some peaks of MgO are present. The differences in the percentage of MgO phase are difficult to perceive in the patterns.

Shown in Fig.8(a) is the surface morphology of the samples sintered for 0.5h. As we can see, the reaction between Mg and B is incomplete. The big grains could not disappear completely. Meanwhile, a large number of small grains have become visible in the grain boundaries. It reveals that the grains are not well connected in the surface for the sample sintered for short time. Some dark grey and light grey impurity phases can be seen for the sample sintered for 0.5h, see Fig.8(b). The energy spectrum analysis showed that the dark one is the B-rich phase (Fig.9) and the light one is the magnetism oxidation compound (Fig.10). However, the grains of the sample sintered for 1h are equiaxial, fine and well-connected, see Fig.8(c). It only has a few small-sized impurity phases, see Fig.8(d). Although the grains are fine as well for the sample sintered for 3h, see Fig.8(e), a great many existing impurities would apparently deteriorate its  $J_c$  performance as shown in Fig.8(f). It indicates undue shorter or longer holding time lead to much more impurity phases and inferior microstructures.

Shown in Fig.11 are magnetization-field loops for samples sintered for different times.  $J_c(H)$  was deduced from the hysteresis loops using the Bean model, see Fig. 12. The sample sintered for 1h has a significantly higher  $J_c$  and than other samples in the magnetic field due to its optimum microstructure. The  $H_{irr}$  value is about 6.3T at 15K, as determined from the closure of hysteresis loops with a criterion of  $J_c = 10^2 A/cm^2$ . The differences in  $J_c$  among them increase with field. The sample sintered for 0.5 and 3h shows a steep drop in  $J_c$  at higher fields ( $H > 4T$  and  $T = 15K$ ). It indicates both columnar grains and excessive impurity phases lead to the bad grain connectivity and weak flux pinning, especially in high magnetic field.

## 4 Summary

In conclusion, the high- $J_c$  MgB<sub>2</sub> bulks were prepared by short-time high energy ball milling. The introduction of impurities (especially oxygen) during the ball-milling process was minimized. A close relation among microstructure, impurities and superconducting properties with the synthesis parameters was detected. The irreversibility field of the optimum sample reaches 6.3T at 15K and  $J_c$  is high around  $1.7 \times 10^6$  A/cm<sup>2</sup> (15K, 0.59T) at 15K in 0.59T. The improved pinning of this material seems to be caused by enhanced grain boundary pinning provided by the large number of grain boundaries in the sample. Another crucial point during preparation of MgB<sub>2</sub> is to avoid weak-link-like behavior at grain boundaries due to a non-superconducting surface layer of magnetism oxidation or B-rich compounds.

## 5 ACKNOWLEDGMENT

This work was partially supported by National Natural Science Foundation project (grant 50472099) and National 973 project (grant 2006CB601004).

## References

- [1] D.C.Larbalestier, L. D. Cooley, M. O. Rikel, A. A. Polyanskii, J. Jiang, S. Patnaik, X. Y. Cai, D.M. Feldman, A. Gurevich, A.A. Squitieri, M.T. Naus, C. B. Eom, E.E. Hellstrom, R. J. Cava, K.A. Regan, N. Rogadao, M. A. Hayward, T. He, J. S. Slusky, P. Khalifah, K. Inumaru, and M. Haas, *Nature* **410**(2001)186.
- [2] A. Yamamoto, J. Shimoyama, S. Ueda, Y.Katsura, S. Horii and K. Kishio, *Supercond. Sci. Technol.* **18**(2005) 116.
- [3] A. Gumbel, J. Eckert, G. Fuchs, K. Nenkov, K. H. Muller and L. Schultz, *Appl. Phys. Lett.* **80**(2002) 2725.
- [4] Y. Bugoslavsky, G. K. Perkins, X. Qi, L. F. Cohen, and A. D. Caplin, *Nature* **410**(2001)563.
- [5] G. Giunchi, S. Ceresara, G. Ripamonti, A. DiZenobio, S. Rossi, S. Chiarelli, M. Spadoni, R. Wesche, P. L. Bruzzone, *Supercond. Sci. Technol.* **16**(2003) 285.
- [6] L. Civale, A. Serquis, D. L. Hammon, J. Y. Coulter, X. Z. Liao, Y. T. Zhu, T. Holesinger, D. E. Peterson, and F. M. Mueller, *IEEE Applied Superconductivity, ASC proceedings, Houston (2002)*.

- [7] H. L. Suo, C. Beneduce, M. Dhall, N. Musolino, J. Y. Genoud, and R. Flükiger, *Appl. Phys. Lett.* 79, 3116 (2001).
- [8] S. X. Dou, J. Horvat, S. Soltanian, X. L. Wang, M. J. Qin, H. K. Liu, and P. G. Munroe, *cond-mat/0208215* (12 Aug 2002).
- [9] H. Fujii, H. Kumakura, and K. Togano, *J. Mat. Res.* 17, 2339 (2002).
- [10] R. Flükiger, H. L. Suo, N. Musolino, C. Beneduce, P. Toulemonde, P. Lezza, *Physica C* 385, 286 (2003).

## Figure captions

Fig.1 XRD patterns of MgB<sub>2</sub> bulks sintered at (a)650 °C, (b) 700 °C, (c)750 °C and (d) 800 °C. Peaks of MgB<sub>2</sub> and MgO are marked by solid circles and squares, respectively.

Fig.2 The SEM photograph of the MgB<sub>2</sub> bulks sintered at different temperatures: (a)650 °C× 15,000 (b)650 °C× 4,000 (c)700 °C× 15,000 (d)700 °C× 4,000 (e)750 °C× 15,000 (f)750 °C× 4,000 (g)800 °C× 15,000 and (h)800 °C× 4,000.

Fig.3 The EDX analysis of the second phase in the sample sintered at 650 °C.

Fig.4 The AC Magnetic susceptibility as a function of temperature of MgB<sub>2</sub> bulks. A constant magnetic field of 1Oe was applied.

Fig.5 Magnetization  $M$  as a function of magnetic field  $H$  at 10K for the samples sintered at different temperatures.

Fig.6 Magnetization critical current density  $J_c$  as a function of magnetic field  $H$  at 10K for the samples sintered at different temperatures.

Fig.7 The XRD patterns of MgB<sub>2</sub> sintered at 750 °C for different holding times. Peaks of MgB<sub>2</sub> and MgO are marked by solid circles and squares, respectively.

Fig.8 The SEM photograph of the MgB<sub>2</sub> bulks sintered for different holding times:(a)0.5h× 15,000(b)0.5h× 4,000 (c)1h× 15,000(d)1h× 4,000 (e)3h× 15,000 and (f)3h× 4,000.

Fig. 9 The EDX analysis of dark gray second phase in the 0.5h sintered sample.

Fig.10 The EDX analysis of light gray second phase in the 0.5h sintered sample.

Fig.11 Magnetization  $M$  as a function of magnetic field  $H$  at 15K for samples sintered for different holding times.

Fig.12 Magnetization critical current density  $J_c$  as a function of magnetic field  $H$  at 15 K for the samples sintered for different holding times.

Fig.1

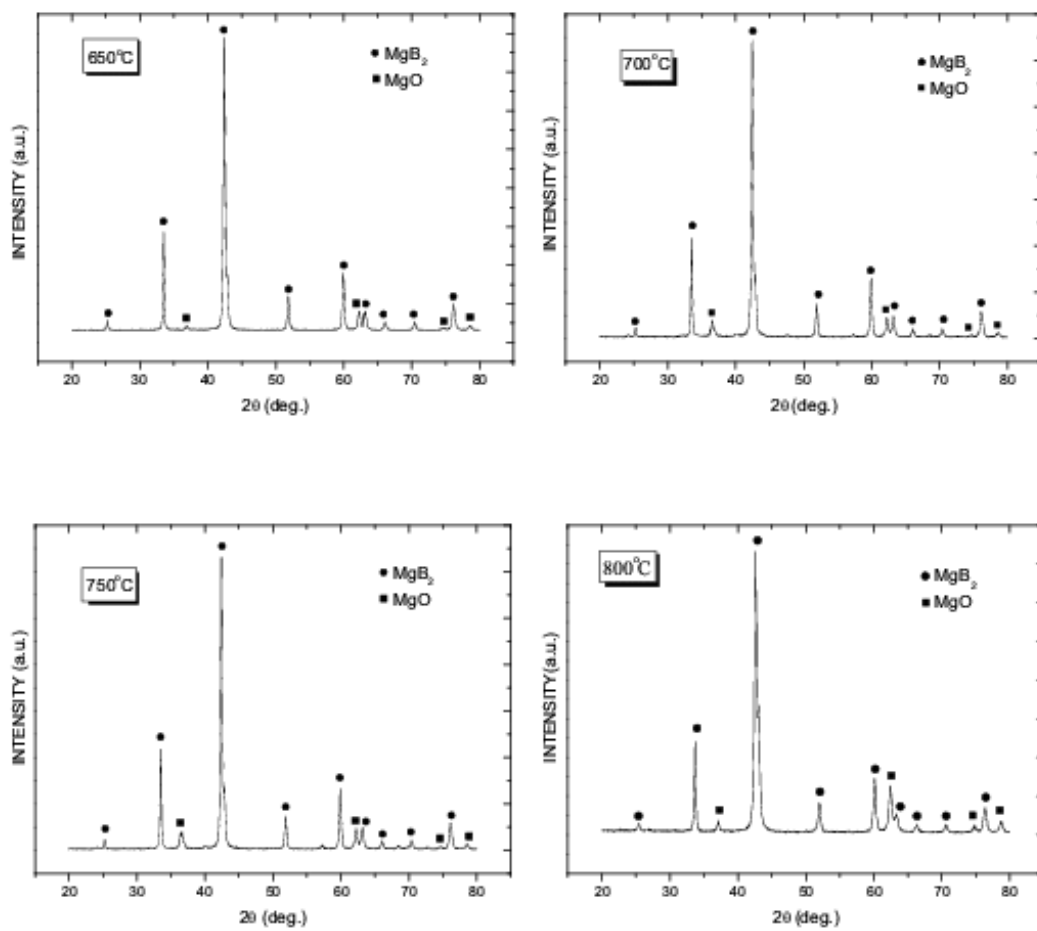


Fig.2

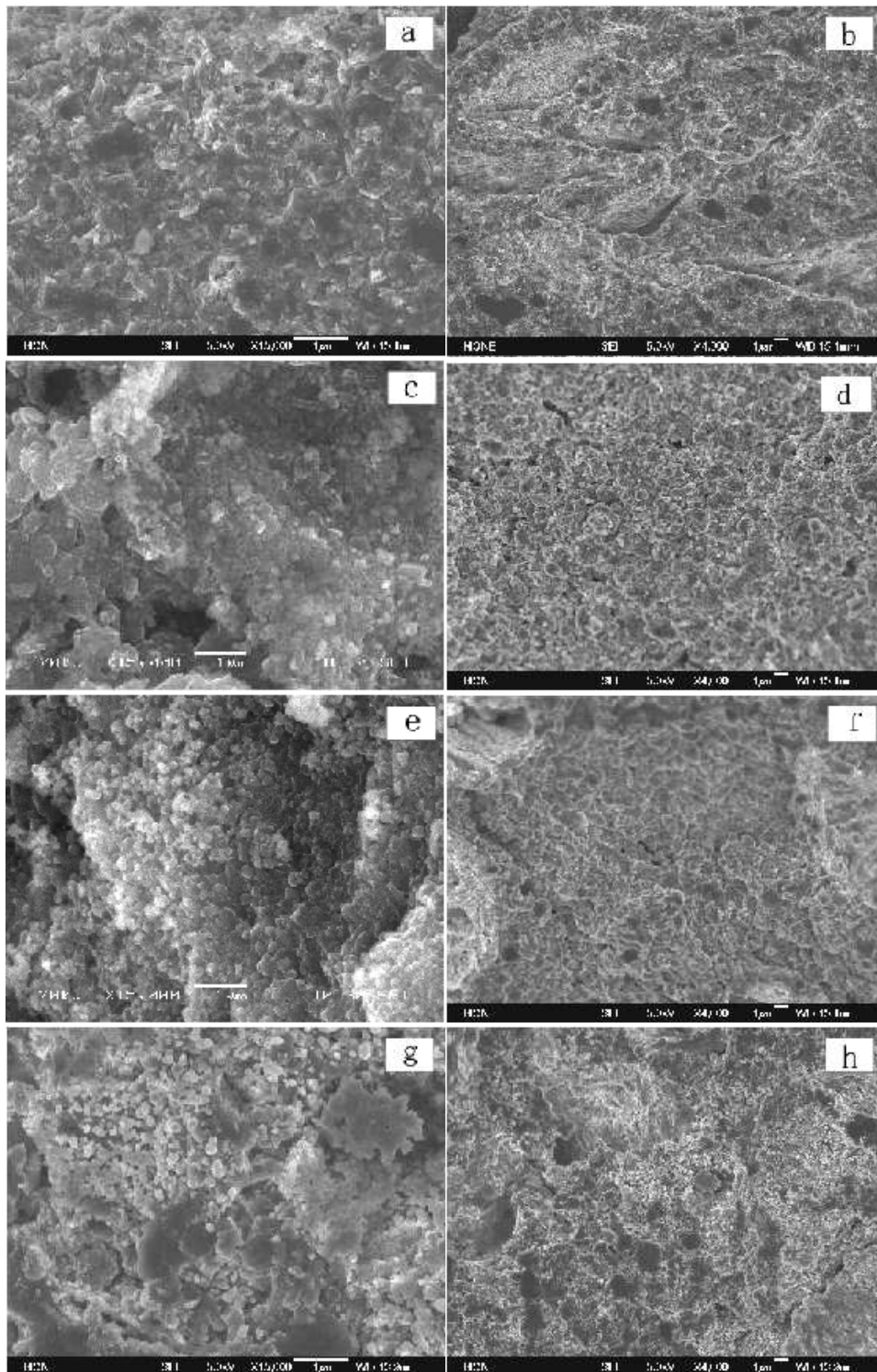
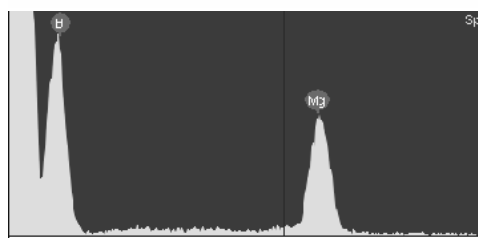
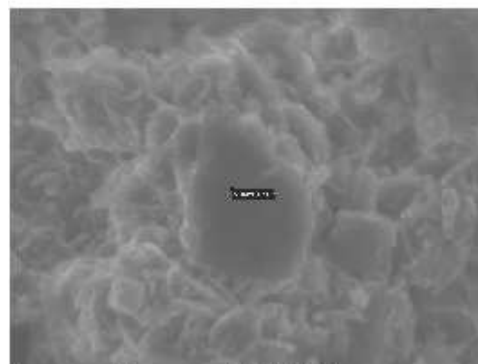


Fig.3



Full Scan 308 cts Cursor: 1.108 keV (16 cts)

Element	Weight%	Atomic%
B K	96.29	98.32
Mg K	3.71	1.68
Totals	100.00	

Fig.4

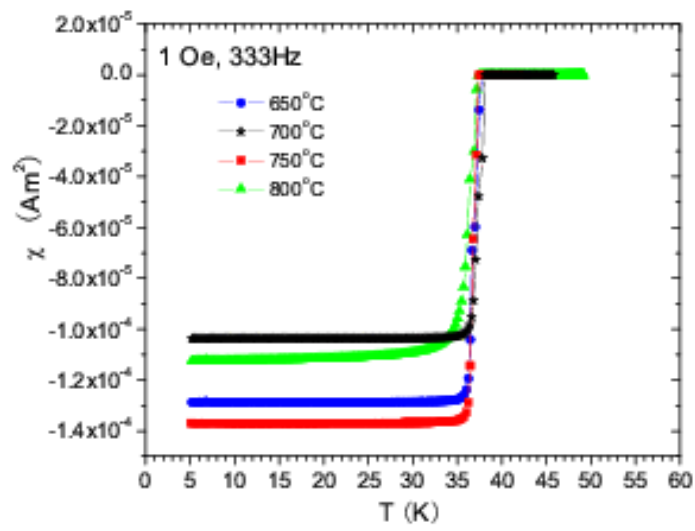


Fig.5

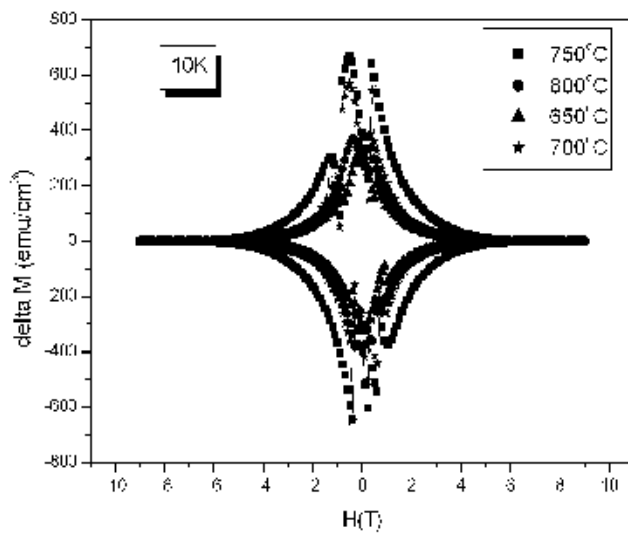


Fig.6

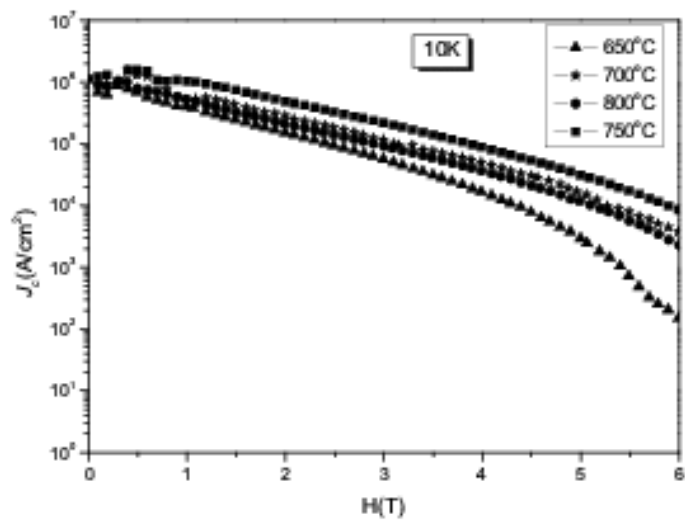


Fig.7

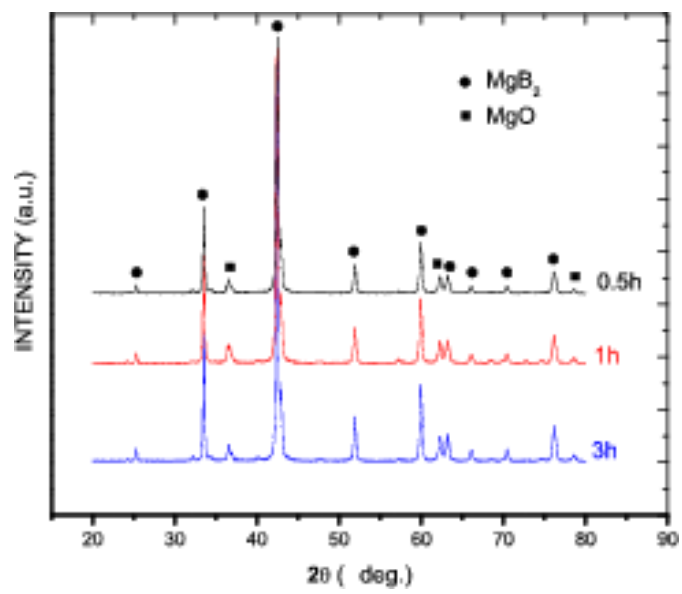


Fig.8

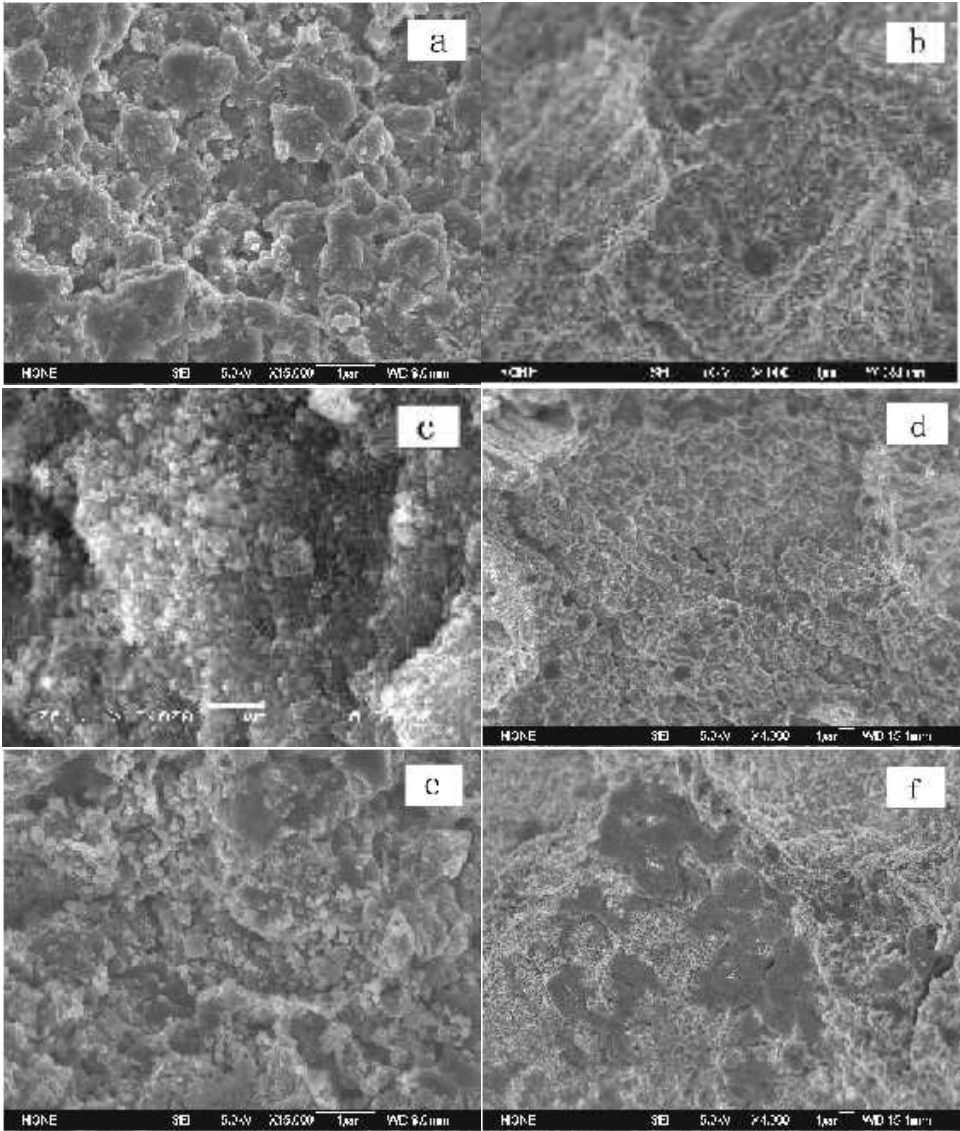
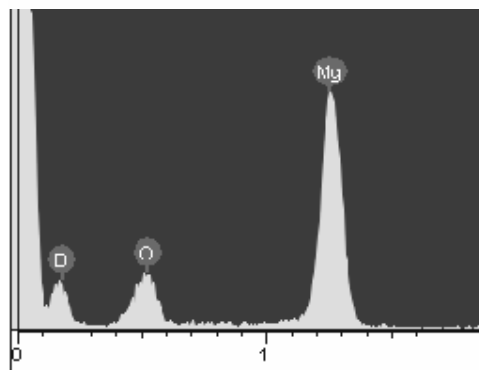
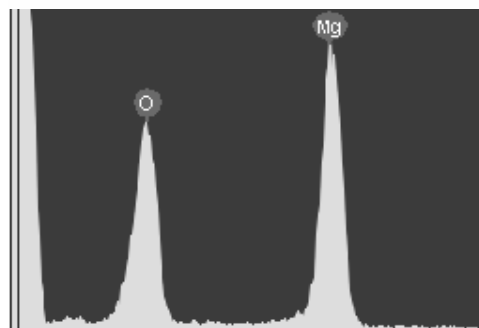


Fig.9



Element	Weight%	Atomic%
B K	71.54	81.16
O K	17.09	13.10
Mg K	11.37	5.73
Totals	100.00	

Fig.10



Full Scale 752 cts Cursor: 0.000 keV

Element	Weight%	Atomic%
O K	57.19	67.30
Mg K	42.81	33.10
Total	100.00	

Fig.11

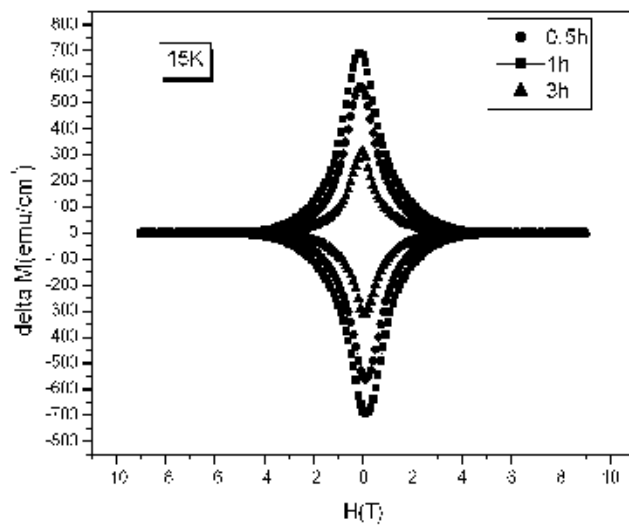


Fig.12

